Raman-Mediated Nonlinear Interactions in Silicon Waveguides: Copropagating and Counterpropagating Pulses

Chethiya Meghawarna Dissanayake, Ivan Dmitrievich Rukhlenko, Malin Premaratne, *Senior Member, IEEE*, and Govind P. Agrawal, *Fellow, IEEE*

***Abstract*—This letter focuses on interaction of copropagating and counterpropagating pulses inside silicon-on-insulator waveguides using finite-difference time-domain (FDTD) simulations. To the best of our knowledge, this is the first time that copropagating and counterpropagation regimes have been analyzed and compared within an extended FDTD model that takes into account linear dispersion of silicon as well as the effect of stimulated Raman scattering. Our analysis shows unambiguously that the second-order Stokes and anti-Stokes sidebands of sufficiently high intensities can develop from noise when the two pulses are copropagating, but these sidebands are absent owing to an inherent phase mismatch when these pulses counterpropagate. We study the evolution of interacting pulses in the temporal and frequency domains and compare the FDTD results with those obtained by integrating a generalized nonlinear Schrödinger equation.**

***Index Terms*—Coherent anti-Stokes Raman scattering, cross-phase modulation, finite-difference time-domain (FDTD) method, four-wave mixing (FWM), linear dispersion, silicon-on-insulator (SOI) waveguides, stimulated Raman scattering (SRS).**

I. Introduction

TODAY, photonics and electronics technologies are rapidly converging towards a silicon-based monolithic technology because of recent realization of many novel optical applications using silicon photonic wires [1]–[3]. Silicon is deemed crucial for such a marriage of distinct technologies because it exhibits a strong nonlinear response that include processes such as stimulated Raman scattering (SRS) and the optical Kerr effect. Also, because of the high refractive index of silicon, it is easy to confine optical modes tightly within a silicon-on-insulator (SOI) waveguide [4]. Unfortunately, the ability to harness the benefits of SRS and the Kerr effect in SOI waveguides are usually hampered by the detrimental effects such as two-photon absorption (TPA), free-carrier absorption (FCA), and free-carrier dispersion (FCD). These effects are especially strong within the standard telecommunication window. For this reason, realization of any chip-scale silicon photonics devices tailored for telecom applications requires extensive theoretical and experimental efforts [2], [3].

Given that general nonlinear solutions can be found for active silicon waveguides only under very specific conditions [5], it is essential to perform detailed numerical simulations to gain a clear insight into the interplay of nonlinearities and to optimize the device design. The well-established, finite-difference time-domain (FDTD) technique is preferred for such detailed simulations over the popular split-step Fourier method [7] because the FDTD scheme allows one to directly solve the electromagnetic field equations with minimal assumptions. Most importantly, the FDTD method provides an accurate and general framework to study propagation of ultrashort pulses, without resorting to the widely deployed, slowly varying envelope approximation. The first FDTD model describing single pulse propagation in SOI waveguides was developed by Suzuki [8]. In the present letter, we extend Suzuki's original scheme by modifying it to account for SRS and linear dispersive effects. This extended model is then used to study the evolution of two picosecond pulses that may propagate through the SOI waveguide in the same or opposite directions. To compare the copropagating and counterpropagating regimes, we assume that pulse lengths are comparable to the waveguide length. After analyzing the impact of different nonlinear effects on pulse interaction, we compare our conclusions with the results in [8] as well as with the theoretical predictions based on the split-step Fourier method [2], [9], [10].

II. FDTD Model for SOI Waveguides

The source-free Maxwell equations for the electric and magnetic fields form the basis for the FDTD analysis of pulse propagation inside an SOI waveguide [6]

$$\nabla \times \mathbf{E} = -\mu_0 \frac{\partial \mathbf{H}}{\partial t}, \quad \nabla \times \mathbf{H} = \frac{\partial \mathbf{D}}{\partial t}.$$

The electric field of an arbitrary optical pulse train containing $\mathcal{N}$ pulses, polarized along the unit vector $\mathbf{e}$, has the form

$$\mathbf{E}(\mathbf{r},t) = \mathbf{e}\sum_{j=1}^{\mathcal{N}} A_j(\mathbf{r},t)\exp(-i\omega_j t) + \text{c.c.}$$

where ω_j is the carrier frequency and $A_j(\mathbf{r},t)$ is the temporal envelope and of the jth pulse. Inside the SOI waveguide, the electric displacement vector $\mathbf{D}$ can be resolved as $\mathbf{D} = \varepsilon_0\mathbf{E} +$

Manuscript received February 04, 2009; revised June 05, 2009. First published July 21, 2009; current version published September 11, 2009. This work was supported by the Australian Research Council through Discovery Grant DP0877232. The work of G. P. Agrawal was also supported by the NSF award ECCS-0801772.

C. M. Dissanayake, I. D. Rukhlenko, and M. Premaratne are with the Advanced Computing and Simulation Laboratory (AXL), Department of Electrical and Computer Systems Engineering, Monash University, Clayton, Victoria 3800, Australia (e-mail: chethiya.dissanayake@eng.monash.edu.au; ivan.rukhlenko@eng.monash.edu.au; malin@eng.monash.edu.au).

G. P. Agrawal is with the Institute of Optics, University of Rochester, Rochester, NY 14627-0186 USA (e-mail: gpa@optics.rochester.edu).

Color versions of one or more of the figures in this letter are available online at http://ieeexplore.ieee.org.

Digital Object Identifier 10.1109/LPT.2009.2027132

$\mathbf{P}$, where the polarization vector $\mathbf{P}$ consists of the linear part $\mathbf{P}_{\rm L}$, and nonlinear contributions arising from the Raman (R), the Kerr (K), TPA, FCA and FCD effects, i.e.,

$$\mathbf{P} = \mathbf{P}_{\rm L} + \mathbf{P}_{\rm R} + \mathbf{P}_{\rm K} + \mathbf{P}_{\rm TPA} + \mathbf{P}_{\rm FCA} + \mathbf{P}_{\rm FCD}.$$

In order to relate various polarizations to the electric field, we need to consider specific models governing the underlying physics. We assume that the pulse-train spectrum lies in the range from 150 to 250 THz which includes the 1.55-μm telecommunication window. The linear dispersion of silicon can then be included by using the following Sellmeier-type equation [10]:

$$\tilde{\mathbf{P}}_{\rm L} = \varepsilon_0 \left(\frac{a\omega_a^2}{\omega_a^2 - \omega^2} + \frac{b\omega_b^2}{\omega_b^2 - \omega^2} + i\frac{cn_0\alpha}{\omega} \right) \tilde{\mathbf{E}} \qquad (1)$$

where $a = 9.733$, $b = 0.936$, $\omega_a = 1032.49$ THz, $\omega_b = 817.28$ THz, and a tilde represents the Fourier transform. The last term in this equation was added to account for linear absorption through the loss coefficient α. In this term, c is the speed of light in vacuum and n_0 is the effective refractive index of the optical mode supported by the SOI waveguide. The Raman polarization can be written as $\mathbf{P}_{\rm R} = \varepsilon_0 \chi_{\rm R} \mathbf{E}$, where $\chi_{\rm R}$ is the Raman susceptibility. In our simulations, we have adopted the classical model of SRS [11] which leads to the following equation for $\chi_{\rm R}(\mathbf{r}, t)$ [3]:

$$\frac{\partial^2 \chi_{\rm R}}{\partial t^2} + \gamma_{\rm R} \frac{\partial \chi_{\rm R}}{\partial t} + \Omega_{\rm R}^2 \chi_{\rm R} = \gamma_{\rm R} \Omega_{\rm R} \xi_{\rm R} |\mathbf{E}|^2$$

where $\gamma_{\rm R} = 106$ GHz is the full-width at half-maximum (FWHM) of the Raman-gain spectrum, $\Omega_{\rm R} = 15.6$ THz is the Raman shift, and $\xi_{\rm R} = 11.2 \times 10^{-18}$ m^2/V^2 for silicon. Compared with the response time of SRS, the response times of TPA and the Kerr effect are so much smaller that these effects can be considered almost instantaneous. The corresponding polarizations are given by [8]

$$\mathbf{P}_{\rm K} = \varepsilon_0 \varepsilon_2 |\mathbf{E}|^2 \mathbf{E}, \quad \tilde{\mathbf{P}}_{\rm TPA} = \frac{ic^2}{2\omega} \varepsilon_0^2 n_0^2 \beta_{\rm TPA} |\tilde{\mathbf{E}}|^2 \tilde{\mathbf{E}} \qquad (2)$$

where $\varepsilon_2 = 1.72 \times 10^{-19}$ m^2/V^2 is the Kerr permittivity and $\beta_{\rm TPA} = 0.9$ cm/GW is the TPA coefficient.

To include the impact of free carriers created through TPA, we take the carrier density N to be the same for electrons and holes. Assuming that FCA and FCD can be treated as nearly instantaneous, we use the following empirical relations [1]:

$$\tilde{\mathbf{P}}_{\rm FCA} = i\varepsilon_0 n_0 (c/\omega) \Delta\alpha_{\rm FC} \tilde{\mathbf{E}}, \quad \tilde{\mathbf{P}}_{\rm FCD} = 2\varepsilon_0 n_0 \Delta n_{\rm FC} \tilde{\mathbf{E}}. \qquad (3)$$

Here, $\Delta\alpha_{\rm FC} = \sigma(\omega_0/\omega)^2 N$ with $\omega_0 = 2\pi c/\lambda_0$, $\lambda_0 = 1550$ nm, $\sigma = 1.45 \times 10^{-17}$ cm^2, and $\Delta n_{\rm FC} = -(8.8 \times 10^{-4} N^{0.2} + 8.5) N^{0.8} (\omega_0/\omega)^2 \times 10^{-18}$ (N in units of cm^{-3}). Finally, the density of free carriers is obtained by solving the rate equation [2]

$$\frac{\partial N}{\partial t} \approx -\frac{N}{\tau_c} + \frac{c^2 \varepsilon_0^2 n_0^2}{8\hbar\omega_p} \beta_{\rm TPA} |\mathbf{E}|^4$$

where τ_c is the effective carrier lifetime and ω_p is the frequency of the strongest input pulse. After converting (1)–(3) to the time domain, we solved Maxwell's equations with the standard FDTD method [6]. The results for the special case of two interacting pulses are discussed in the next Section.

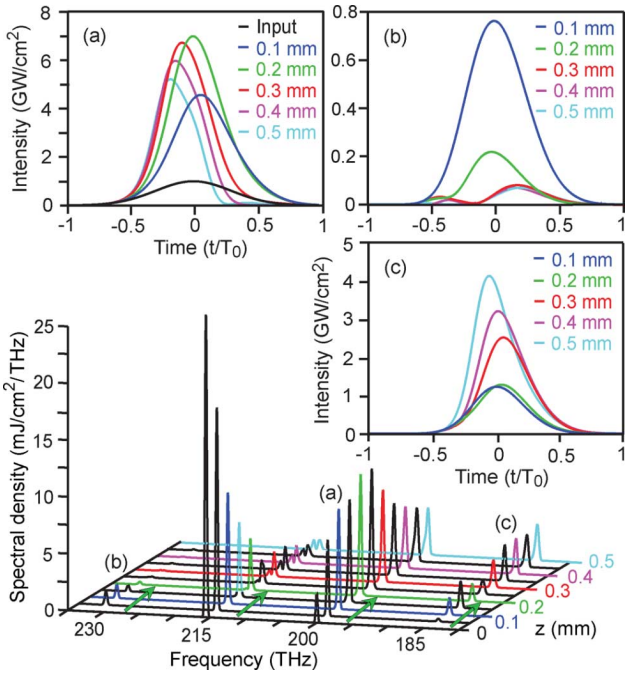

Fig. 1. Spectra evolution of two copropagating Gaussian pulses separated by Raman frequency shift. Insets show the detailed intensity profiles of (a) signal, (b) upper-, and (c) lower-sidebands for different propagation distances z.

III. Simulation Results

We consider two Gaussian pulses with FWHMs of $T_0 = 2$ ps propagating inside a single-mode SOI waveguide with a cross section area 425×200 nm^2. We set the waveguide length equal to 0.5 mm, so that it is close to the pulse length cT_0/n_0. This allows for a fair comparison of copropagating and counterpropagation regimes. The input peak intensities for the pump pulse at $\omega_1 = 215.6$ THz and the signal pulse at $\omega_2 = 200$ THz are set to 10 and 1 GW/cm^2, respectively. Other simulation parameters employed are: $n_0 = 3.039$, $\alpha = 0.22$ dB/cm, and $\tau_c = 0.8$ ns.

Fig. 1 shows the numerically calculated spectra of copropagating pulses at different distances inside the SOI waveguide. One can clearly see the formation of two additional spectral sidebands (near 184 and 231 THz) from the third-order nonlinear process of four-wave mixing (FWM). Since the pump-signal detuning is equal to the Raman shift, the nonlinear phonon susceptibility $\chi_{\rm R}$ contributes to the FWM leading to the coherent anti-Stokes Raman scattering [12]. Once formed, two spectral components together with pump and signal are also subjected to multiple Raman-mediated energy transfer processes. It is significant that intensity of the upper sideband [Fig. 1, inset (b)] is stronger than that of the lower sideband [inset (c)] near $z = 0.05$ mm. However, owing to the rapid depletion by SRS, the upper sideband becomes negligible close to the waveguide output, whereas the lower sideband competes with the signal [inset (a)] all along the waveguide and even comprises around 80% of the signal peak intensity at $z = 0.5$ mm. It should also be noted that the asymmetry of the signal and the lower-sideband intensity profiles are not

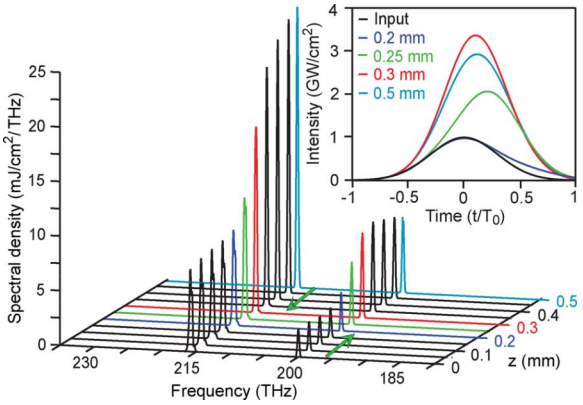

Fig. 2. Spectra evolution of two counterpropagating Gaussian pulses separated by Raman frequency shift. Inset shows the detailed intensity profiles of signal for different propagation distances z.

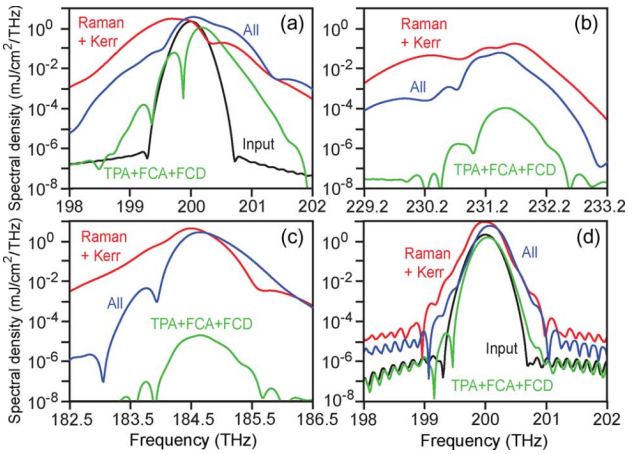

Fig. 3. Signal [(a) and (d)], lower- (b), and upper-sideband (c) spectra showing the impact of different nonlinear effects at the end of the 0.5-mm SOI waveguide. The spectra (a)–(c) correspond to Fig. 1; the spectra (d) corresponds to Fig. 2.

due to FCA (which is relatively weak when $T_0 \ll \tau_c$ [2]) but rather due to the cross-phase modulation and complex impact of FCD on the FWM process. In addition to FCD, the efficiency of FWM is affected by the linear dispersion, which cause a considerable phase mismatch among the interacting waves.

The spectral evolution of counterpropagating pump and signal pulses is presented in Fig. 2. In contrast to the copropagating regime, the second-order spectral sidebands are absent because of an unavoidable phase mismatch between the pump and the signal [12]. As a result, the signal remains nearly symmetric during propagation, as illustrated by the inset in Fig. 2. It is notable that the output signal energies in copropagating and counterpropagation regimes are nearly equal despite the fact that durations of pulse interaction in these regimes differ roughly by a factor of 2. Such an equalization of energy conversion efficiency in the two propagation regimes becomes possible because the pump energy is distributed between the signal and the second-order Stokes sideband in the copropagation regime.

Fig. 3 illustrates the impact of different nonlinear effects on the spectra of signal and other sidebands seen in Figs. 1 and 2. The black curves show the spectra of the input signal. The green curves include only the effects of TPA, FCA, and FCD, while the red curves include only the Raman and Kerr effects. Lastly, the blue curves show the spectra when all these effects occur simultaneously. One can see that the signal spectral distortion (e.g., broadening) represented by green, red, or blue curves is much smaller in the counterpropagation regime [inset (d)] from that in the copropagation regime [inset (a)]. The spectra presented in the insets (b) and (c) show that the efficiency of FWM is dominated by the Raman and Kerr effects, whereas FWM induced by TPA, FCA, and FCD is relatively small. In spite of this feature, the effect of FCD on the signal spectra is quite strong, as can be seen by comparing the blue and red curves. Finally, it is worth noting that the FCD-induced blue shift, which is known to be one of the characteristic features exhibited by a single pulse spectrum in SOI waveguides [8], [10], is still present in copropagation regime but is nearly compensated by the red shifts associated with the Raman and Kerr effects.

IV. Conclusion

We presented an extended FDTD model to account for Raman-mediated pulse interactions when two short optical pulses, separated in frequency by the Raman shift, propagate through a silicon waveguide. Using this model, we studied in detail the interaction of two copropagating and counterpropagating Gaussian pulses. We found that the generation of second-order Stokes sideband substantially reduces the signal gain in the copropagation regime. It was also found that, when widths of the pulses are comparable with the length of the waveguide, the broadening of signal spectrum is much smaller in the counterpropagation regime compared with that occurring in the copropagation regime. These features indicate that counterpropagation may be a more suitable mode of SOI-based Raman amplifiers.

References

[1] R. Soref, "The past, present, and future of silicon photonics," *IEEE J. Sel. Topics Quantum Electron.*, vol. 12, no. 6, pt. 2, pp. 1678–1687, Nov./Dec. 2006.

[2] Q. Lin, O. J. Painter, and G. P. Agrawal, "Nonlinear optical phenomena in silicon waveguides: Modeling and applications," *Opt. Express*, vol. 15, pp. 16604–16644, 2007.

[3] B. Jalali, V. Raghunathan, D. Dimitropoulos, and O. Boyraz, "Raman-based silicon photonics," *IEEE J. Sel. Topics Quantum Electron.*, vol. 12, no. 3, pp. 412–421, May/Jun. 2006.

[4] H. K. Tsang and Y. Liu, "Nonlinear optical properties of silicon waveguides," *Semicond. Sci. Technol.*, vol. 23, pp. 064007(1)–064007(9), 2008.

[5] I. Rukhlenko, M. Premaratne, C. Dissanayake, and G. P. Agrawal, "Continuous-wave Raman amplification in silicon waveguides: Beyond the undepleted pump approximation," *Opt. Lett.*, vol. 34, pp. 536–538, 2009.

[6] A. Taflove and S. C. Hagness, *Computational Electrodynamics: The Finite-Difference Time-Domain Method*. Norwood, MA: Artech House, 2005.

[7] G. P. Agrawal, *Nonlinear Fiber Optics*, 4th ed. San Diego, CA: Academic, 2007.

[8] N. Suzuki, "FDTD analysis of two-photon absorption and free-carrier absorption in Si high-index-contrast waveguides," *J. Lightw. Technol.*, vol. 25, no. 9, pp. 2495–2501, Sep. 2007.

[9] X. Chen, N. C. Panoiu, and R. M. Osgood, Jr., "Theory of Raman-mediated pulsed amplification in silicon-wire waveguides," *IEEE J. Quantum Electron.*, vol. 42, no. 2, pp. 160–170, Feb. 2006.

[10] L. Yin, Q. Lin, and G. P. Agrawal, "Soliton fission and supercontinuum generation in silicon waveguides," *Opt. Lett.*, vol. 32, pp. 391–393, 2007.

[11] R. W. Boyd, *Nonlinear Optics*, 2nd ed. San Diego, CA: Academic, 2003.

[12] R. Claps, V. Raghunathan, D. Dimitropoulos, and B. Jalali, "Anti-stokes Raman conversion in silicon waveguides," *Opt. Express*, vol. 11, pp. 2862–2872, 2003.